Computer Science Department of The University of Auckland
CITR at Tamaki Campus (http://www.tcs.auckland.ac.nz**)**

CS-TR-150 / CITR-TR-8 July 1997

Sound Analysis of 3D Objects Based on Digitized Data

Reinhard Klette*

Abstract

The report reviews selected results in the field of geometrical measurements and reconstructions of 3D objects (i.e. simply-connected compact sets of points) based on gridding techniques. Two soundness properties of approaches are discussed with respect to the selected grid resolution: *convergence* and *convergence towards the "true" value*. The existence of sound multigrid approaches is discussed for problems as (1) volume and surface area measurement for Jordan sets (i.e. 3D objects bounded by Jordan surfaces), (2) approximations of planes based on sampled data, (3) surface reconstructions based on gradient information, and (4) surface recovery by solving a (special) linear differential equation system. The paper concludes with a brief discussion of arising digital or computational geometry problems relevant to the discussed subjects.

* The University of Auckland, Tamaki Campus, Computing and Information Technology Research, Computer Vision Unit, Auckland, New Zealand

Sound Analysis of 3D Objects Based on Digitized Data

Reinhard Klette

Computing and Information Technology Research, Tamaki Campus
Computer Science Department, University of Auckland
Auckland, New Zealand

Abstract. The report reviews selected results in the field of geometrical measurements and reconstructions of simply-connected compact sets of points in $\mathbf{R}^3$ which have internal points (i.e. a special class of 3D objects) based on gridding techniques. Two soundness properties of approaches are discussed with respect to the selected grid resolution: *convergence* and *convergence towards the "true" value*. The existence of sound multigrid approaches is discussed for problems as (1) volume and surface area measurement for Jordan sets (i.e. 3D objects bounded by Jordan surfaces), (2) approximations of planes based on sampled data, (3) surface reconstructions based on gradient information, and (4) surface recovery by solving a (special) linear differential equation system. The report concludes with a brief discussion of arising digital or computational geometry problems relevant to the discussed subjects.

1 Introduction

This report deals with approximations and representations of objects (sets, surfaces, faces, planes etc.) in three-dimensional (3D) space that are initially given by discrete data arrays. The application background is image analysis of three-dimensional objects based on given digitized data. The input information may be either a *voxel data set*, where *voxel* stands for *volume element* which is the sample value at a grid point, or it may be one or several digitized projections of real-world scenes. Example application areas are biomedical 3D image analysis, or industrial surface inspection, respectively. The analysis task is directed towards reconstructing or analyzing an unknown 3D object.

To be precise, an object in the 3D Euclidean space $\mathbf{R}^3$ is a connected compact set. A *compact set* is characterised by two properties: any infinite sequence of points of this set contains a convergent subsequence, and the set is closed with respect to the topology of the Euclidean space. Lateron in this report we restrict our objects of interest on sets bounded by a *Jordan surface*, or on sets which are just a single *Jordan face* in 3D. An object in three-dimensional space may be characterised to be either one-dimensional, two-dimensional, or three-dimensional. A one-dimensional object in $\mathbf{R}^3$ is a curve. A two-dimensional object in $\mathbf{R}^3$ has no internal points (with respect to the 3D topology), i.e. it is a surface in $\mathbf{R}^3$. A 3D object is a connected compact set in $\mathbf{R}^3$ which has internal points with respect to the 3D topology. Furthermore we will assume that a *3D object* in this report is also simply-connected. A *simply-connected set* is homeomorphic to a unit ball.

This report is not a general review. It is based on subjective selections of relevant topics and results (without citing proofs) in the area of geometrical measurements and surface reconstructions based on gridding techniques.

1.1 Soundness Properties

The length of a diagonal of a square with side length a can not be measured via the length of a piecewise constant function because the total length of the piecewise constant function is always $2a$ independent of the number or the size of the steps, and does not converge towards $a\sqrt{2}$ if the step-size goes to zero. This is a popular example of the following problem: assume that a real-world object is given and we have only some sampled or digitized data about this 3D object. What is the appropriate method to calculate a specific feature of this object, or to represent it? Does the method ensure that progress in technology (higher resolution of cameras, more storage, digital images of larger size etc.) will lead to "improved" results?

Sound multigrid measurement approaches for areas in 2D, or for volumes in 3D are not especially hard to specify (the 3D case will be discussed below). For the "diagonal of a square" example above the size of the area below the "diagonal" staircase function will converge towards the size of the triangle defined by two sides of the square and the diagonal if the step size goes to zero. However the sound measurement of perimeters in 2D, or of surface areas in 3D are more difficult problems.

Digital geometry techniques or computational geometry algorithms may be used to represent and analyze the given discrete data. The chosen technique should be sound with respect to the *general measurement or representation problem* that discrete measurements (sampled data) are given about a certain object, and that this object has to be represented in a certain data structure (specific features, specific approximative representations etc.).

We consider the following two soundness properties of measurement or reconstruction techniques in this report:

CONVERGENCE: Data acquisition at higher spatial resolutions should lead to a certain type of convergence (as uniform, pointwise etc.) for the values of measured features, or for the calculated representations such as reconstructed planes, straight lines, surfaces etc.

PROPER VALUE: Convergence should be towards the "true" value, the "true" data etc.

The first soundness property requires a proof of a certain type of convergence. The diagonal in the *staircase example* above is always $2a$, i.e. it trivally converges.

The proof of the second soundness property (convergence towards the "true" value) is often more difficult than a proof of a certain type of convergence. Besides the mathematical difficulty of such a proof it requires in application areas as computer vision or image analysis also at first a fundamental problem analysis: what is actually the "true data", the so-called *ground truth*? The objects of interest may be well-defined by a deterministical, a fuzzy or a statistical mathematical model, or characterised by a certain degree of objective or subjective uncertainty.

Often the "true" data is unknown in applications of image analysis. In image analysis the 3D object is given in a certain discrete form as, e.g., a (discrete) voxel data set, and must be analyzed based on this discrete information which is characterized by a given grid resolution. Sometimes we may also utilise a certain a-priori geometric model (as polyhedron, or "smooth surface object") of the unknown 3D object. However we will focus on the general case where just the given discrete information (voxels, gradient values at grid point position etc.) specifies the input. For example, many imaging processes such as Computer Tomography (CT), Magnetic Resonance Imaging (MRI) or Confocal Microscopy (CSLM), provide a series of aligned planar scans which together comprise a special voxel data set, a *voxel data cube*. Some microscope image analysis processes are based on digitized slices of objects where at first the obtained images have to be aligned. However, assuming correct alignment also in these cases such a voxel data cube is given describing a certain 3D object. The object Θ of interest, represented in this data cube, is normally given as a fuzzy set and not defined by a Jordan surface. Fig. 1 intends to visualise such a "fuzzy situation" of capturing real objects.

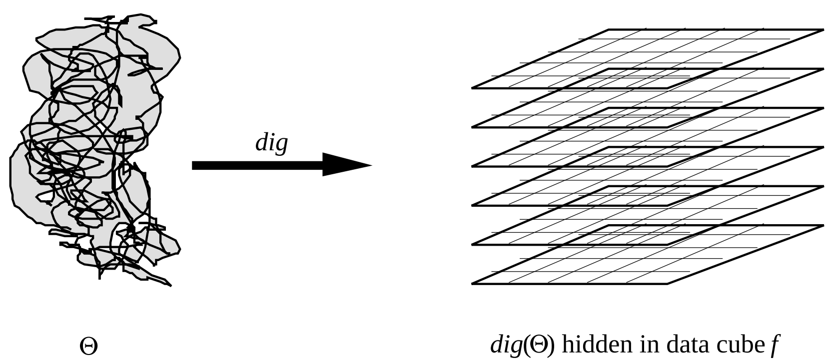

Fig. 1. An unknown real-world object Θ , the ground truth, is represented after image acquisition as $dig(\Theta)$, and this information is "hidden" within a voxel data cube f of labeled grid points.

Higher resolutions during image acquisition may allow to restrict the range of possible (subjective) object interpretations, i.e. to improve the understanding of the "hidden" 3D object. This is an important argument for the approach discussed in this report.

The study of soundness properties of suggested measurement or reconstruction techniques can be based on synthetic input data as a solution for generating "ground truth" simulating real input data. However such experiments are always just case studies for a specific type of hypothetical input data.

The ideal solution is the mathematical modeling of the measurement or reconstruction problem where the truth is defined in general mathematical terms. An evaluation approach based on a general mathematical model of an assumed measurement and representation problem does not require experiments with real or synthetic input data (besides that, such experiments may be useful to illustrate or to validate), but it is restricted to a certain class of precisely definable problems. In such a mathematical model we have not to discuss difficulties with specifying a "ground truth" because there is only one truth in such a model.

In deterministic models the problem of convergence is always considered with respect to convergence towards a uniquely defined true value, without statistical distributions or fuzzy uncertainties. This report discusses such well-defined deterministic situations.

What is the "true" surface area in case of mathematically defined 3D objects? There must be a unique answer to this question. Indeed this question is easy to answer for objects as planar, polygonal faces. It is easy to model a plane, a polygonal face or a straight line. The diagonal in the staircase example above has length $a\sqrt{2}$. But what about curved objects as an ellipsoid in general form (assuming three different values for the three radii of such an ellipsoid) modelling "curved objects" in the real world?

Fortunately integration and differentiation techniques for modeling surfaces in 3D Euclidean space were already studied in mathematics since the 19th century, see, e.g., No. 109 in [19], and provide proper approaches for modeling and measuring of object surfaces. But note that "simple" objects as an ellipsoid in general form are already quite difficult with respect to the determination of an analytical surface area formula, and numeric calculations are often prefered in mathematical software systems.

1.2 Jordan Faces

C. Jordan (1838 Lyon - 1922 Paris) is already famous in the image analysis literature for his curve theorem often cited for separations in 2D Euclidean space. A generalization of this Jordan curve theorem is also valid for specific sets of points in 3D space allowing a more specific definition of 3D objects which we will call *Jordan sets*.

However at first we start the definition of a general surface model for simply-connected compact 3D objects by assuming a segmentation of the 3D object surface into several faces.

Definition 1. (Jordan Face): A **Jordan face F** in 3D Euclidean space $\mathbf{R}^3$ is a set of points $\mathbf{F} \subseteq \mathbf{R}^3$ in parameteric form $\mathbf{F} = \mathbf{F_B}(\varphi, \psi, \chi)$ where $\mathbf{B} \subseteq \mathbf{R}^2$ is a simply-connected compact set and φ, ψ, and χ are three functions differentiable for all positions (u, v) in $\mathbf{B}$, such that

$$\mathbf{F_B}(\varphi, \psi, \chi) = \{(x, y, z) : x = \varphi(u, v) \wedge y = \psi(u, v) \wedge z = \chi(u, v) \wedge (u, v) \in \mathbf{B}\},$$

and for which it is assumed that each point in $\mathbf{F_B}(\varphi, \psi, \chi)$ is defined by exactly one point $(u, v) \in \mathbf{B}$, and that the rank of the matrix of the first derivatives

$$\begin{pmatrix} \varphi_u & \psi_u & \chi_u \\ \varphi_v & \psi_v & \chi_v \end{pmatrix}$$

is equal to two for all positions $(u, v) \in \mathbf{B}$.

From this definition it follows that at each position $\mathbf{b} = (u, v)$ at least one of the three subdeterminants

$$A = \begin{vmatrix} \psi_u & \chi_u \\ \psi_v & \chi_v \end{vmatrix}, \quad B = \begin{vmatrix} \chi_u & \varphi_u \\ \chi_v & \varphi_v \end{vmatrix}, \quad \text{and} \quad C = \begin{vmatrix} \varphi_u & \psi_u \\ \varphi_v & \psi_v \end{vmatrix}$$

is not equal to zero. These subdeterminants may be used to define the area $J_{area}(\mathbf{F})$ of face $\mathbf{F}$ as follows

$$J_{area}(\mathbf{F}) = \int\limits_{\mathbf{B}} \sqrt{A^2 + B^2 + C^2} d\mathbf{b}$$

assuming that $\mathbf{F}$ is measurable (see Definition 3 below).

For example assume any simply-connected planar compact face $\mathbf{F}$. Then $\mathbf{B}$ may be chosen parallel to the $\mathbf{F}$ plane, with $\varphi(u, v) = const$, $\psi(u, v) = u$, and $\chi(u, v) = v$. The rank of the corresponding matrix

$$\begin{pmatrix} 0 & 1 & 0 \\ 0 & 0 & 1 \end{pmatrix}$$

is two and the equation

$$J_{area}(\mathbf{F}) = \int\limits_{\mathbf{B}} d\mathbf{b} = J_{area}(\mathbf{B})$$

reduces the 3D measurement problem to a 2D measurement problem. It follows that any simply-connected planar compact set $\mathbf{F}$ is a Jordan face according to the definition above, and it is measurable if its 2D projection is measurable.

The measurability definition [19] of Jordan faces $\mathbf{F} = \mathbf{F_B}(\varphi, \psi, \chi)$ is based on a triangulation of a bounded superset $\mathbf{B}_1$ of $\mathbf{B}$ satisfying $\mathbf{B} \subseteq I(\mathbf{B}_1)$, where $I(\mathbf{B}_1)$ denotes the 2D *interior* of the set $\mathbf{B}_1$, and the first order derivatives of the functions φ, ψ, χ exist and they are continuous in $I(\mathbf{B}_1)$. Formally this means that φ, ψ, $\chi \in C^{(1)}(I(\mathbf{B}_1))$. In No. 108 of [19] it is shown that the angles α of such triangulations (of the base sets of the resulting polyhedral faces) have to satisfy the constraint $\alpha < 2\pi/3$ (independently shown by *O. Hölder* in 1882, *G. Peano* in 1890, and *H. A. Schwarz* in 1890) to avoid inaccurate surface value calculations for curved surfaces. This might also be cited as a remarkable result for triangulations in modern computer graphics.

Definition 2. (Triangular Subdivision): Let $\mathbf{B}_1 \subseteq \mathbf{R}^2$ be a simply-connected compact set with $\mathbf{B} \subseteq I(\mathbf{B}_1)$ and assume an angle ω with $0 < \omega < \pi/3$. Then any network Z of triangles completely covering $\mathbf{B}_1$ and satisfying the following two properties,

(i) all angles of triangles in Z are less or equal to $\pi - \omega$, and

(ii) for all triangles in Z having at least one point in common with set $\mathbf{B}$ it holds that all three corner points are in set $\mathbf{B}_1$,

is called a **triangular subdivision** Z of $\mathbf{B}_1$ with respect to $\mathbf{B}$.

Definition 3. (Measurable Jordan Face): Let $\mathbf{F} = \mathbf{F_B}(\varphi, \psi, \chi)$ be a Jordan face as defined above. Assume that there exists a simply-connected compact set $\mathbf{B}_1 \subseteq \mathbf{R}^2$ such that $\mathbf{B} \subseteq I(\mathbf{B}_1)$, the functions φ, ψ, χ are in $C^{(1)}(I(\mathbf{B}_1))$, and there exists a sequence Z_1, Z_2, Z_3, ... of triangular subdivisions of $\mathbf{B}_1$ with respect to $\mathbf{B}$ such that

$$a_t \to 0$$

where a_t denotes the maximum length of any side of any triangle in the subdivision Z_t. Each triangular subdivision Z of $\mathbf{B}_1$ with respect to $\mathbf{B}$ defines a polyhedral approximation $\mathbf{F}(Z)$ of the given Jordan face $\mathbf{F} = \mathbf{F_B}(\varphi, \psi, \chi)$, forming an infinite sequence of polyhedral approximations

$$\mathbf{F}(Z_1), \quad \mathbf{F}(Z_2), \quad \mathbf{F}(Z_3), \ldots$$

having well-defined surface areas

$$J_{area}(\mathbf{F}(Z_1)), \quad J_{area}(\mathbf{F}(Z_2)), \quad J_{area}(\mathbf{F}(Z_3)), \ldots$$

The Jordan face $\mathbf{F}$ is **measurable** if it has a bounded surface area

$$J_{area}(\mathbf{F}) = \sup_t \; J_{area}(\mathbf{F}(Z_t)).$$

Theorem 4. (Jordan Face Area Theorem): *For a measurable Jordan face* $\mathbf{F} = \mathbf{F_B}(\varphi, \psi, \chi)$ *it holds*

$$J_{area}(\mathbf{F}) = \int_{\mathbf{B}} \sqrt{A^2 + B^2 + C^2} \; d\mathbf{b}$$

independent of the chosen parametrization $\mathbf{B}$, φ, ψ, *where* A, B *and* C *are the subdeterminants as defined above.*

This theorem is a historic result about Jordan faces, and a complete proof may be found in [19]. It points out that a proof about the measurability of a given Jordan face (and its value of the surface area) may be based on just one selected parametrization of this face, and on just one selected triangular subdivision satisfying the angle constraint as specified in Definition 2.

1.3 Jordan Surfaces

A single Jordan face can not form a complete surface of a non-trivial (i.e. having a non-zero volume value) 3D object. Because of the assumed property that each point in $\mathbf{F_B}(\varphi, \psi, \chi)$ is defined by exactly one point $(u, v) \in \mathbf{B}$ it follows that at least two faces are necessary to obtain a closed surface of a non-trivial 3D object. Furthermore, the assumed $C^{(1)}$ property of functions φ, ψ, and χ allows no discontinuities within a single Jordan face, as it appears at edges of polyhedral objects. A *polyhedron* is a 3D object where the 3D interior is simply-connected, and the boundary is the union of a finite number of simply-connected planar compact sets. A single Jordan face can not in general be "an edge" (i.e. two incident non-complanar faces of the boundary) of a polyhedron.

Definition 5. (Jordan Set, Jordan Surface, Surface Area): A **Jordan set** is a simply-connected compact set $\Theta \subset \mathbf{R}^3$ the boundary of which is the union of a finite number of measurable Jordan faces $\mathbf{F}_1$, $\mathbf{F}_2$, ..., $\mathbf{F}_n$. A **Jordan surface** $\mathbf{S} = S(\Theta)$ is the boundary $\partial\Theta$ of a Jordan set Θ, i.e.

$$\mathbf{S} = \mathbf{F}_1 \cup \mathbf{F}_2 \cup ... \cup \mathbf{F}_n .$$

Assuming that the 2D interiors of the sets $\mathbf{F}_t$ are pairwise disjoint the **surface area** of $\mathbf{S}$ is defined as

$$J_{area}(\mathbf{S}) = J_{area}(\mathbf{F}_1) + J_{area}(\mathbf{F}_2) + ... + J_{area}(\mathbf{F}_n) .$$

The open set $I(\Theta) = \Theta - \partial\Theta$ is the 3D *interior* of this Jordan set Θ. Note that a Jordan set is always homeomorphic to a unit ball, and a Jordan surface is always homeomorphic to the unit sphere, i.e. the surface of the unit ball. Each polyhedron is a Jordan set and many curved 3D objects may be classified to be Jordan sets.

A *smooth Jordan set* has a surface which possesses a uniquely defined tangent plane in each of its surface points. Note that this is not necessarily the case for a union of measurable Jordan faces. The following Theorem holds for smooth, and also for non-smooth Jordan surfaces.

Theorem 6. (Jordan Surface Theorem): *Any surface* $\mathbf{S}$ *of a Jordan set subdivides the* $\mathbf{R}^3$ *into three disjoint sets* $\mathbf{I}$, *the set* $\mathbf{S}$ *itself, and a set* $\mathbf{E} = \mathbf{R}^3 - (\mathbf{S} \cup \mathbf{I})$ *where* $\mathbf{I}$ *and* $\mathbf{E}$ *are open sets with* $\partial\mathbf{I} = \partial\mathbf{E} = \mathbf{S}$.

The open set $\mathbf{E} = E(\mathbf{S})$ is the 3D *exterior* of the Jordan set $\mathbf{S} \cup \mathbf{I}$. "Going from $\mathbf{I}$ to $\mathbf{E}$ " means that we have "to leave $\mathbf{I}$ " by passing through its boundary $\partial\mathbf{I} = \mathbf{S}$, i.e. any curve starting in $\mathbf{I}$ and ending in $\mathbf{E}$ intersects the given surface $\mathbf{S}$ at least once. A Jordan surface specifies a separation in 3D Euclidean space as a Jordan curve does in 2D Euclidean space.

So far the surface area of a Jordan set (from now on our more specialised model of a 3D object) is specified in this report, and further features (as volumes $J_{volume}(\Theta)$, centroids, moments, potentials etc. of Jordan sets Θ) may be uniquely defined following classical mathematical texts as [19]. Such features are the "true data" in deterministic mathematical models which may be discussed with respect of multigrid convergence of algorithms or approaches.

Image acquisition may be modeled at a certain level of abstraction as a mapping of a given Jordan set, which is surrounded by further Jordan sets, into a digital space. Techniques generating a voxel data cube are mapping the whole Jordan set and its surrounding set(s) into a certain grid. Techniques based on projective mappings produce some projective images of the given Jordan set within specified image grids. The next Section deals with the digitization process related to the first approach of 3D image acquisition.

Note that the treatment of 3D objects with fuzzy surfaces would require a non-trivial extension of the Jordan set model, of the following digitization models etc.

2 Object Digitization

Grids (not only orthogonal ones) were introduced by *C. Jordan* and *G. Peano* around 1890 for defining measurable sets (now known as the *Jordan*, or the *Jordan-Peano area* of a set). The formation of *digital geometry* as a fundamental subject in image analysis by *A. Rosenfeld* around 1965 was an important step for establishing a scientific approach in image analysis in contrast to an application oriented approach. The mapping of "real objects" into grid point sets was always an inherent problem in digital geometry, and several models are in use as an abstraction of the image acquisition processes.

2.1 Orthogonal Grids at Different Resolutions

We assume labeled points $\mathbf{p}$ in the 3D orthogonal grid, with integer coordinates (i, j, k) at grid point positions, to be the raw representation of the digitized object data, where $1 \leq i, j, k \leq N$. In the case of *binary labels* we assume either $f(i, j, k) = 0$ or $f(i, j, k) = 1$, and 0 means that the grid point is "not in the object', and 1 means that the grid point is "inside of the object". In the case of *fuzzy labels* $f(i, j, k) = u$ in the interval $[0, 1]$ it is normally intended that label u means that a grid point is an object point "with fuzzy weight u." For example assume grey value images and a threshold T for separating object from background image values. Then u may be defined by a certain normalized distance between the current image value and the threshold value T.

A voxel data cube f may be described as being an $N \times N \times N$ set of labeled grid points. We consider only the binary 3D cubic grid model in this report. Orthogonal grids subdivide the space $\mathbf{R}^3$ with different resolutions, say 2^{-r} with $r = 0, 1, 2, ...$, where each *grid point* (i, j, k) having integer coordinates represents a *cell*

$$\mathbf{C}_r\,(i, j, k) = \left\{(x, y, z) \in \mathbf{R}^3 :\ x \in [i]_r \wedge y \in [j]_r \wedge z \in [k]_r\right\}$$

in $\mathbf{R}^3$, with

$$[m]_r = \left\{x :\ \left(m - \tfrac{1}{2}\right) \cdot 2^{-r} \leq x \leq \left(m + \tfrac{1}{2}\right) \cdot 2^{-r}\right\}$$

for an integer m. Each cell is a Jordan set, it has a volume of

$$J_{volume}\left(\mathbf{C}_r\,(i, j, k)\right) = 2^{-3r},$$

its surface consists of at least six Jordan faces, and its surface area equals

$$J_{area}\left(\mathbf{C}_r\,(i, j, k)\right) = 6 \cdot 2^{-2r}.$$

In relation to the fixed coordinate scales of the reference space $\mathbf{R}^3$ we define $\mathbf{Z}_r^3$ to be the *r-grid point set* where each r-grid point (i, j, k) is the midpoint of the cell $\mathbf{C}_r\,(i, j, k)$:

Definition 7. (Grid Point Set of Specified Resolution): The **r-grid point structure** $\left[\mathbf{Z}^3, \xi_r\right]$ consists of the base set $\mathbf{Z}^3$ of all grid points in 3D, and an **interpretation** ξ_r which maps an r-grid point (i, j, k) into $\mathbf{R}^3$, onto the midpoint of the cell $\mathbf{C}_r\,(i, j, k)$, for $r = 0, 1, 2, ...$ Let $\mathbf{Z}_r^3 = \left\{\xi_r\,(\mathbf{p}) :\quad \mathbf{p} \in \mathbf{Z}^3\right\}$.

It follows that $\mathbf{Z}_r = \{m \cdot 2^{-r} :\ m \in \mathbf{Z}\}$. An r-grid point $\mathbf{p}$ may be specified by its *name* $(i, j, k) \in \mathbf{Z}^3$ or by its *geometrical location* $\xi_r\,(\mathbf{p})$.

This dual approach allows the discussion of general grid terminology as neighborhoods or connectedness on the base of names of r-grid points in $\mathbf{Z}^3$, and geometric properties of refined grids on the base of their geometric interpretations in $\mathbf{Z}_r^3$.

All $N_r \times N_r \times N_r$ r-grid points $\mathbf{p} = (i, j, k)$ correspond to a finite subset of the infinite base set $\mathbf{Z}^3$. Assuming that the overall geometrically represented cube in $\mathbf{R}^3$, the *universe*

$$\mathbf{C}_{uni} = \left\{(x, y, z) \in \mathbf{R}^3 :\ 0 \leq x, y, z \leq N_0 + 1\right\}$$

is constant for a certain image analysis situation it follows that a larger resolution parameter r means a larger resolution $N_r = 2^r \cdot (N_0 + 1) - 1$, and vice versa.

Grid point spaces may be defined based on such a specified r-grid point structure, and these spaces are fundamental for multi-dimensional image analysis problems, see [24]. Neighborhood relations are introduced on the base set $\mathbf{Z}^3$ to specify adjacency or connectedness properties. For $0 \leq t \leq 2$ and $t \in \mathbf{Z}$, let

$$fix_t = \{(x_1, x_2, x_3) : \forall i\,(1 \leq i \leq 3 \rightarrow x_i \in \{-1, 0, +1\}) \wedge card\,\{i : x_i = 0\} = t\}$$

be a subset of the surface of a three-dimensional cube $[-1,+1]^3$. For example, $(1,0,1) \in fix_1$ is in the surface but not a corner of this cube, and $fix_0 = \{-1,+1\}^3$ represents the set of all corners of this cube. Assuming that any grid point $\mathbf{p} \in \mathbf{Z}^3$ also denotes a *grid vector*, from the origin to the grid point $\mathbf{p}$, it follows that the addition of two grid points is uniquely defined.

Definition 8. (Neighborhood and Adjacency of Grid Points): For $\mathbf{p} \in \mathbf{Z}^3$ and $0 \leq t \leq 2$, the set

$$\eta_t(\mathbf{p}) = \mathbf{p} + \bigcup_{j=t}^{2} fix_j$$

denotes the **t-neighborhood** of point $\mathbf{p}$. For $\mathbf{q} \in \eta_t(\mathbf{p})$ we say that $\mathbf{q}$ is a **t-neighbor** of $\mathbf{p}$, and that $\mathbf{p}$ and $\mathbf{q}$ are **t-adjacent**.

The relation of t-adjacency is irreflexive and symmetric. The transitive closure of this relation defines *t-connectedness* for sets of grid points in 3D. For $\mathbf{p} \in \mathbf{Z}^3$ and $0 \leq t \leq 2$ we have

$$card(\eta_t(\mathbf{p})) = \sum_{j=t}^{2} 2^{3-j} \binom{3}{j},$$

i.e. $card(\eta_2(\mathbf{p})) = 6$, $card(\eta_1(\mathbf{p})) = 18$, and $card(\eta_0(\mathbf{p})) = 26$, accordingly the notions *6-, 18-*, or *26-neighborhood* or *6-, 18-*, or *26-connectedness* are common in digital 3D image analysis. A *homogeneous grid point net* $[\mathbf{Z}^3, \eta_t]$ can be defined, representing an infinite undirected labeled graph, with vertex set $\mathbf{Z}^3$ and edge set

$$\{(\mathbf{p},\mathbf{q}) : \mathbf{p} \in \mathbf{Z}^3 \wedge \mathbf{q} \in \eta_t(\mathbf{p})\}.$$

Nets of grid points are studied in [32]. The *homogeneous net of r-grid points* $[\mathbf{Z}^3, \eta_t, \xi_r]$ is also characterized by the interpretation ξ_r.

2.2 Digitization Schemes

A digitization mapping can be specified as a model of the given physical image acquisition process. This allows the use of real-world test objects for evaluation. The exact modeling of imaging processes such as confocal microscopy or MRI is a complex task, and evaluations based on statistical data (i.e. populations of test objects, e.g. calibration spheres [3]) are proper techniques to achieve meaningful results. We will not follow that way in this report. Each image acquisition process (MRI, confocal microscopy etc.) would need its own specification. We prefer a more general approach.

A general digitization model specifies a certain mapping of given planes, straight lines, Jordan sets, etc. contained in the universal cube $\mathbf{C}_{uni}$, into an orthogonal grid of size $N_r \times N_r \times N_r$. See for example [10] for a general scheme to define such models for n-dimensional spaces but without modeling refined resolutions.

A common (but in relation to hardware devices, idealized) model for digitizing oriented real arcs in $\mathbf{R}^2$ into the grid $\mathbf{Z}_r^2$ may be described as follows (the so-called *grid intersection digitization* [14, 23]). For any intersection point of arc γ with a grid line defined by two points (i, j_1), (i, j_2) or (i_1, j), (i_2, j) in $\mathbf{Z}_r^2$ the closest (according to Euclidean metric) grid point in $\mathbf{Z}_r^2$ to this intersection point in $\mathbf{R}^2$ will be chosen as an element of the *digital image* of γ; if the intersection point is the midpoint of a grid edge then the point on the right side of γ (according to its orientation) is chosen. In [8] a similar grid intersection scheme was used for the digitization of straight lines in $\mathbf{R}^3$.

Using this intersection scheme, the straight line (orientation with increase of parameter a)

$$\gamma = \left\{ \left(a, 2^{-(r+1)} + a \right) : a \in \mathbf{R} \right\}$$

in $\mathbf{R}^2$ will always, for any $r \geq 0$, lead to the digital image

$$\mathbf{A}_r = \{(q, q) : q \in \mathbf{Z}_r\},$$

for example. If in the case where the intersection point is a midpoint of a grid edge the point on the left side of γ is chosen, then the digital image

$$\mathbf{B}_r = \{(q, q+1) : q \in \mathbf{Z}_r\}$$

would be the digitization result. If in this midpoint case the point closest to the origin is chosen the digital image

$$\mathbf{A}_r \cup \mathbf{B}_r$$

would result.

We return to the 3D case. To avoid such "midpoint discussions" for curves in 3D it can be suggested that we assume for arcs γ in $\mathbf{R}^3$ that for any crossing with a grid plane

$$x_i = q \in \mathbf{Z}_r$$

at point $\mathbf{p}$ there is exactly one grid point in $\mathbf{Z}_r^3$ that is the closest grid point to $\mathbf{p}$, for any coordinate axis $1 \leq i \leq 3$. This assumption is violated only by a set of measure zero assuming a straightforward defined measurable space of all arcs in 3D.

Let Π_r^σ be a bounded subset of $\mathbf{R}^3$ containing at least the origin of $\mathbf{R}^3$, for $r = 1, 2, 3, \ldots$ and σ is a metavariable of a name of the given set. Examples for such sets Π_r^σ are

$$\Pi_r^{cube} = \left\{ (x_1, x_2, x_3) : \quad \max_{1 \leq i \leq 3} |x_i| \leq 2^{-r} \right\},$$

$$\Pi_r^{octahedron} = \left\{ (x_1, x_2, x_3) : \quad \max\left\{ |x_1|, |x_2|, |x_3|, \tfrac{1}{2} \sum_{i=1}^{3} |x_i| \right\} \leq 2^{-r} \right\},$$

$$\Pi_r^{sphere} = \left\{ (x_1, x_2, x_3) : \quad \sum_{i=1}^{3} x_i^2 \leq 2^{-2r} \right\}, \text{and}$$

$$\Pi_r^{cross} = \left\{ (x_1, x_2, x_3) : \quad \max_{1 \le i \le 3} |x_i| \ \le 2^{-r} \wedge \exists j \left(1 \le j \le m \wedge x_j = 0\right) \right\},$$

for $r = 1, 2, 3, ...$

Let $\Pi_r^\sigma(\mathbf{q}) = \{\mathbf{q} + \mathbf{p} : \mathbf{p} \in \Pi_r^\sigma\} = \mathbf{q} + \Pi_r^\sigma$ for any point $\mathbf{q} \in \mathbf{R}^3$. For any r-grid point $\mathbf{p} = (i \cdot 2^{-r}, j \cdot 2^{-r}, k \cdot 2^{-r}) \in \mathbf{Z}_r^3$ and $\sigma \in \{octahedron, sphere, cross\}$ it holds that

$$\Pi_r^{cube}(\mathbf{p}) = \mathbf{C}_{r-1}(i, j, k),$$

and the sets $\Pi_r^\sigma(\mathbf{p})$ are subsets of the cell $\mathbf{C}_{r-1}(i, j, k)$.

Furthermore assume that Π_r^σ satisfies the following uniqueness condition that for each point $\mathbf{p} \in \mathbf{R}^3$ there exists at most one grid point $\mathbf{q} \in \mathbf{Z}_r^3$ such that $\mathbf{p} \in \Pi_r^\sigma(\mathbf{q})$. The given example sets satisfy these constraints. It holds that $\mathbf{q} \in \mathbf{Z}_r^3$ is exactly the only one r-grid point in $\Pi_r^\sigma(\mathbf{q})$. We use such a set Π_r^σ as the *domain of influence* of a digitization scheme, where σ specifies the name of the scheme.

Definition 9. (Intersection Digitization): For $\mathbf{p} \in \mathbf{R}^3$, a name σ and $r = 1, 2, 3, ...$ let

$$DIG_r^\sigma(\mathbf{p}) = \begin{cases} \{\mathbf{q}\} & \text{if} \quad \mathbf{q} \in \mathbf{Z}_r^3 \quad \text{and} \quad \mathbf{p} \in \Pi_r^\sigma(\mathbf{q}) \\ \emptyset & \text{otherwise} \end{cases}$$

For a subset Θ of $\mathbf{R}^3$,

$$DIG_r^\sigma(\Theta) = \bigcup_{\mathbf{p} \in \Theta} DIG_r^\sigma(\mathbf{p})$$

denotes the digital image of Θ according to the **intersection digitization mapping** DIG_r^σ.

Corollary 10. *An r-grid point $\mathbf{q} \in \mathbf{Z}_r^3$ is in the digital image $DIG_r^\sigma(\Theta)$ of a set $\Theta \subseteq \mathbf{R}^3$ iff $\Theta \cap \Pi_r^\sigma(\mathbf{q}) \neq \emptyset$.*

The different domains of influence define intersection digitization schemes as DIG_r^{cube}, $DIG_r^{octahedron}$, DIG_r^{sphere}, or DIG_r^{cross}. The scheme DIG_r^{cross} is the *grid-intersection digitization* in 3D. In [4] it is shown that grid-intersection digitization is "a poor choice" for digital curve representation in 3D space and that cube quantization, which leads to 6-connected r-grid points in $\mathbf{Z}_r^3$, should be preferred. The sphere intersection digitization scheme is not suitable for curves since even infinite straight lines can pass between the spheres without intersecting any of them, see Fig. 2.

However for digitizing Jordan sets Θ the use of such intersection digitization schemes may be suggested for consideration. An intersection digitization of a Jordan set Θ leads to a certain r-grid point set which may also be represented as a binary voxel data cube f.

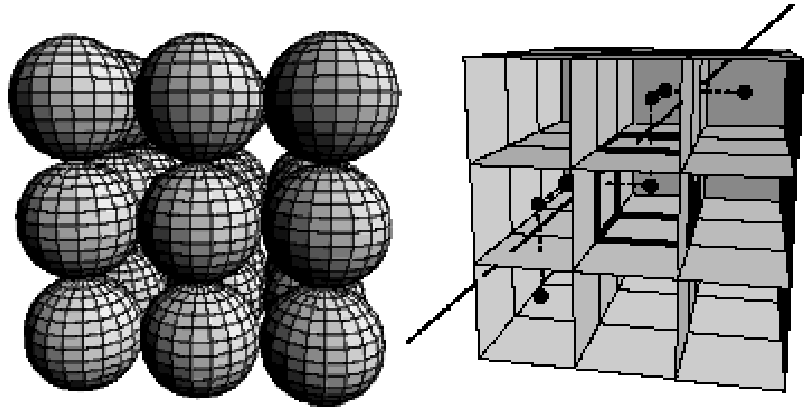

Fig. 2. The generalization of 2D circle intersection digitization to 3D spherical digitization (on the left) allows that infinite straight lines can pass between the spheres without intersecting any of them. However the scheme can be considered for digitizing solid 3D objects. The cube intersection digitization (on the right) maps a straight line into a 6-connected grid-point sequence [4].

Definition 11. (Inclusion Digitization): For a subset Θ of $\mathbf{R}^3$ and a domain of influence Π_r^σ,

$$dig_r^\sigma(\Theta) = \left\{\mathbf{q} \in \mathbf{Z}_r^3 : \quad \Pi_r^\sigma(\mathbf{q}) \subseteq I(\Theta)\right\}$$

denotes the digital image of Θ according to the **inclusion digitization mapping** dig_r^σ.

Examples of inclusion digitization mappings are dig_r^{cube}, dig_r^{cross}, dig_r^{sphere}, and $dig_r^{octahedron}$. The assumed properties of areas of influence lead to the following

Corollary 12. *For any set $\Theta \subset \mathbf{R}^3$ and any domain of influence Π_r^σ it holds that $dig_r^\sigma(\Theta) \subseteq \Theta \cap \mathbf{Z}_r^3 \subseteq DIG_r^\sigma(\Theta)$.*

Following traditional approaches in 2D digital geometry we use DIG_r^{cube} to define an *outer interior* $\mathbf{I}_r^+ = I_r^+(\Theta)$, and dig_r^{cube} to define an *inner interior* $\mathbf{I}_r^- = I_r^-(\Theta)$ of a Jordan set Θ. Let

$$vol_r(\mathbf{G}) = \bigcup_{\mathbf{q}\in\mathbf{G}} \quad \Pi_{r+1}^{cube}(\mathbf{q})$$

where $\mathbf{G}$ denotes a set (of geometric locations) of r-grid points in $\mathbf{Z}_r^3$, and $r = 0, 1, 2, \ldots$. The general definition utilizing arbitrary domains of influence is as follows:

Definition 13. (Inner, Intermediate and Outer Interior): For a subset Θ of $\mathbf{R}^3$ and a domain of influence Π_r^σ,

$$\mathbf{I}_r^{\sigma-} = I_r^{\sigma-}(\Theta) = vol_r\left(dig_r^\sigma(\Theta)\right) \quad \text{and} \quad \mathbf{I}_r^{\sigma+} = I_r^{\sigma+}(\Theta) = vol_r\left(DIG_r^\sigma(\Theta)\right)$$

denote the **inner** and the **outer interior**, respectively, and

$$\mathbf{I}_r = I_r(\Theta) = vol_r\left(\Theta \cap \mathbf{Z}_r^3\right)$$

denotes the **intermediate interior**.

The inner, intermediate, and outer exterior $\mathbf{E}_r^{\sigma-}$, $\mathbf{E}_r$, and $\mathbf{E}_r^{\sigma+}$ could be defined in a similar way. - With Corollary 12 it follows immediately that also these volume data satisfy the monotonicity property of

Corollary 14. *[25] For any set $\Theta \subset \mathbf{R}^3$ and any domain of influence Π_r^σ it holds that $I_r^{\sigma-}(\Theta) \subseteq I_r(\Theta) \subseteq I_r^{\sigma+}(\Theta)$.*

It follows that

$$J_{volume}\left(I_r^{\sigma-}(\Theta)\right) = card\left(dig_r^\sigma(\Theta)\right) \cdot 2^{-3r},$$

$$J_{volume}\left(I_r(\Theta)\right) = card\left(\Theta \cap \mathbf{Z}_r^3\right) \cdot 2^{-3r},$$

and

$$J_{volume}\left(I_r^{\sigma+}(\Theta)\right) = card\left(DIG_r^\sigma(\Theta)\right) \cdot 2^{-3r}$$

are the volumes of these different discrete representations of the given set $\Theta \subset \mathbf{R}^3$, and the surface areas J_{area} of these different discrete representations may be calculated in a similar way adding all the surface areas of faces on the boundaries of the sets $\mathbf{I}_r^{\sigma-}$, $\mathbf{I}_r$, and $\mathbf{I}_r^{\sigma+}$. In the following we omit the domain of influence index σ if the discussion is about the *cube* digitization scheme, i.e. it is $dig_r = dig_r^{cube}$, $\mathbf{I}_r^+ = \mathbf{I}_r^{cube+}$ etc. in what follows.

Theorem 15. (Cube Digitization Theorem): *The proper inclusion $\mathbf{I}_r^- \subset I(\mathbf{I}_r^+)$ holds for any non-empty subset Θ of $\mathbf{R}^3$.*

It follows that $\partial\mathbf{I}_r^- \cap \partial\mathbf{I}_r^+ = \emptyset$. Note that the set $\mathbf{I}_r^-$ may be empty for a non-empty set Θ and a selected resolution r. But the set $\mathbf{I}_r^+$ will always be non-empty for a non-empty set Θ. Fig. 3 illustrates an example of *square* intersection digitization in 2D. Here the polygonal border of this polygon passes on the left exactly through the vertices of cells introducing some extra cells into the outer interior, and it also possesses a "thin spike" ("thin" with respect to the resolution!) on the right generating some cells for the outer interior which are further away from the inner interior. Similar situations may appear for cube intersection digitization in 3D. Examples in the 3D space are illustrated in Fig. 4 and in Fig. 5, where a sphere and a torus (note: this is not a simply-connected object) are used as ground truth, respectively.

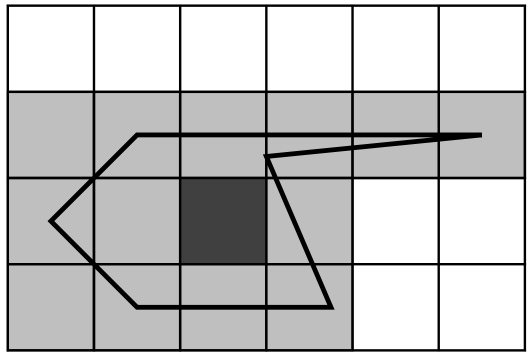

Fig. 3. Cells in 2D showing the inner interior (one cell - dark shaded) and the outer interior (14 cells - light or dark shaded).

3 Convergence Analysis

So far the necessary definitions were given for starting the analysis of such specific 3D image analysis problems as measuring the volume or the surface area of a digitized 3D object, approximating a connected region of given digital surface points by a special explicit face function as, e.g., a plane, calculating height data of an object face which is only given by gradient values at discrete locations, or discrete recovery of a Jordan face as a special solution of a Cauchy problem. The latter two problems are relevant to shape reconstruction, see [11]. The brief discussion of these four situations are different case studies of the general soundness approach if gridding techniques are applied.

3.1 Volume and Surface Area Calculation

We assume as input a finite 6-connected set $\mathbf{G} \subset \mathbf{Z}^3$ of grid points. This set is assumed to be a digital representation of a Jordan set Θ, for a certain resolution parameter r. Therefore it is assumed that $\mathbf{G}$ is geometrically interpreted to be an r-grid point set contained in $\mathbf{Z}_r^3$.

TASK: The task is to calculate the volume and the surface area of Θ based on the available input set $\mathbf{G} \subset \mathbf{Z}_r^3$.

What is methodologically a sound approach for calculating these features satisfying the soundness properties stated in Section 1.1?

The digitization process is modeled as being a *cube* intersection digitization method. Thus the given grid point set $\mathbf{G}$ is identified with an r-grid point rep-

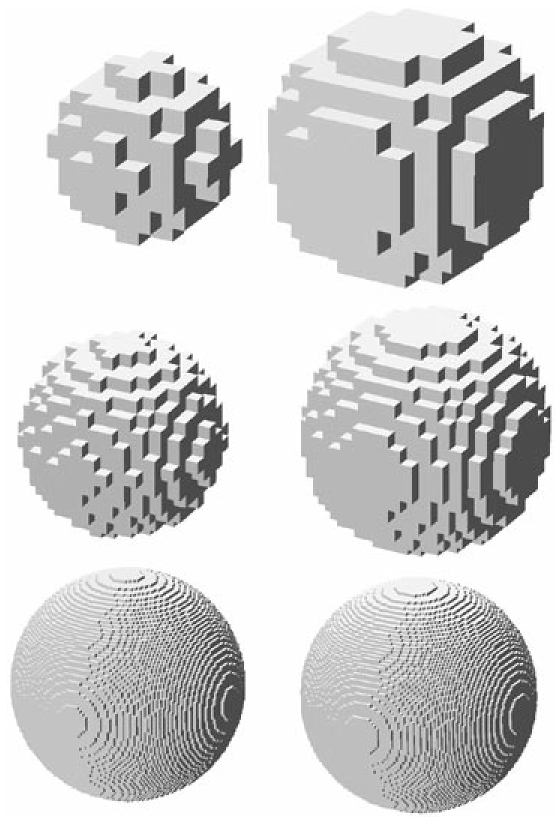

Fig. 4. Inner interiors (on the left) and outer interiors (on the right) of a sphere, i.e. a Jordan set, for three different grid resolutions [7].

resentation $DIG_r(\Theta)$ of the unknown 3D object Θ, and this set defines the inner interior $\mathbf{I}_r^-$. Furthermore we can generate the smallest possible (which is uniquely defined, see the Cube Digitization Theorem above) outer interior $\mathbf{I}_r^+$ by a simple dilation operation on $\mathbf{G}$ using the 26-neighborhood as a structural element (dilation is defined and studied on the set $\mathbf{Z}^3$ of names of r-grid points). This dilation leads to an *expanded set* $\mathbf{G}^+$ which may be considered to be the set $DIG_r(\Theta)$ which finally defines $\mathbf{I}_r^+$. Because the actual shape of set Θ in $\mathbf{R}^3$ is unknown we are not able to suggest an approximation of the intermediate interior $\mathbf{I}_r$.

The volume calculation for the unknown object Θ in $\mathbf{R}^3$ may be based on $J_{volume}(\mathbf{I}_r^-)$ as well as on $J_{volume}(\mathbf{I}_r^+)$, see [25]. Both approaches are sound

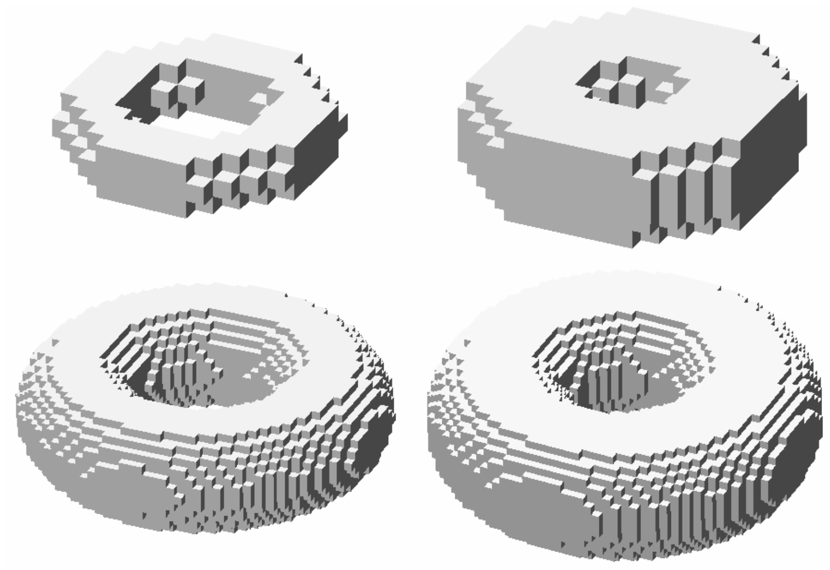

Fig. 5. Inner interiors (on the left) and outer interiors (on the right) of a torus (note: not a Jordan set), for two different grid resolutions [7].

(convergence and convergence towards proper value) for Jordan sets Θ :

Theorem 16. (Volume Measurement Theorem): *For any Jordan set* $\Theta \subset \mathbf{R}^3$ *it holds that*

$$J_{volume}(\Theta) = \sup_{r\to\infty} J_{volume}(\mathbf{I}_r^-) = \inf_{r\to\infty} J_{volume}(\mathbf{I}_r^+),$$

where $\mathbf{G} = dig_r(\Theta)$, $\mathbf{I}_r^- = vol_r(\mathbf{G})$, *and* $\mathbf{I}_r^+ = vol_r(\mathbf{G}^+)$.

Unfortunately such a convergence

$$J_{volume}(\Theta) = \lim_{r\to\infty} J_{volume}(\mathbf{I}_r^-) = \lim_{r\to\infty} J_{volume}(\mathbf{I}_r^+)$$

to the proper value is not true in general for the case of surface area measurement. However a sound measurement procedure for surface areas of Jordan sets was developed in [29]. For explaining this approach we first note that both the inner interior $\mathbf{I}_r^- = vol_r(G)$, and the outer interior $\mathbf{I}_r^+ = vol_r(G^+)$ are polyhedrons in $\mathbf{R}^3$, with $\mathbf{I}_r^- \subset I(\mathbf{I}_r^+)$ (see Cube Digitization Theorem).

Theorem 17. (Minimum Jordan Surface Theorem *[29]* **):** *Assume that* Π_1, Π_2 *are polyhedrons in* $\mathbf{R}^3$ *with* $\Pi_1 \subset I(\Pi_2)$. *Then there exists a uniquely* *defined Jordan surface* $\mathbf{S}$ *in* $\Pi_2 - I(\Pi_1)$ *with minimum surface area, which is the boundary of a certain polyhedron* Π.

The set $\Pi_2 - I(\Pi_1)$ is polyhedral bounded and compact. It follows that the *minimum Jordan surface* $\mathbf{S} = \partial\Pi$ "is between" the inner polyhedral surface $\partial\Pi_1$ and the outer polyhedral surface $\partial\Pi_2$, i.e. $\Pi_1 \subseteq \Pi \subset \Pi_2$.

Corollary 18. *There exists a uniquely defined minimum Jordan surface in the connected compact set* $vol_r(\mathbf{G}^+) - I(vol_r(\mathbf{G}))$.

Starting with a Jordan set Θ, the set $\mathbf{G}$ was defined by resolution r. Thus Θ and r uniquely define a minimum Jordan surface $MJS_r(\Theta)$ having a surface area of $J_{area}(MJS_r(\Theta))$.

For a convex set such as the sphere, the minimum Jordan surface is simply defined by the convex hull of the inner interior.

Theorem 19. (Surface Measurement Theorem *[29]* **):** *For any smooth Jordan set* $\Theta \subset \mathbf{R}^3$ *it holds that*

$$J_{area}(\partial\Theta) = \lim_{r\to\infty} J_{area}(MJS_r(\Theta))$$

where $MJS_r(\Theta)$ *is the uniquely defined minimum Jordan surface for resolution* $r = 0, 1, 2, ...$

The theorem is also valid for Jordan surfaces which possess a finite number of edges. A polyhedron has its surface area well definited. Altogether this specifies a sound (i.e. convergence and convergence towards the proper value) procedure for calculating the surface area of a digitized Jordan set. However the design of time-efficient algorithms for calculating the minimum Jordan surface polyhedron should be an interesting problem in computational geometry where a 6-connected grid point set is given as input. The 2D case of minimum perimeter polygons is treated in [27, 28].

Marching cubes [18] may be considered to define an approximation technique for calculating minimum Jordan surfaces. Each elementary grid cube, defined by eight grid points, is treated according to a look-up table for defining planar surface patches within this elementary grid cube. See [5] for a complete set of marching cubes configurations. The fourteen basic configurations originally suggested by [18] are incomplete. Occasionally they generate "surfaces with holes". The marching cubes algorithm determines the surface by deciding how the surface intersects a given elementary grid cube. A surface can intersect an elementary grid cube in 2^8 different ways, and these can be represented as fourteen major cases with respect to rotational symmetry. Alternatively a method developed by [34] calculates the contour chains immediately without using a look-up table of all 2^8 different cases.

Disambiguities of the marching cube look-up tables are discussed in [33]. A marching tetrahedra algorithm was suggested in [22]. It generates more triangles than the marching cubes algorithm in general. Trilinear interpolation functions were used in [2] for the different basic cases of the marching cubes algorithm. In comparison to the marching cube algorithm [5] the accuracy of the calculated surface area improved by using this trilinear marching cube algorithm, which was confirmed for a few synthetic Jordan faces.

3.2 Approximation of Planes

We assume as input a finite set $\mathbf{G} \subset \mathbf{Z}^3$ of grid points. This set is assumed to be a digital representation of a planar set Θ with non-empty $2D$ interior incident with a plane $\alpha \subset \mathbf{R}^3$. We assume that $\mathbf{G}$ is geometrically interpreted to be an r-grid point set contained in $\mathbf{Z}_r^3$. Concerning the digitization method assume that the plane α is digitized using an intersection digitization scheme DIG_r^{below} in which the first grid points "below the given plane" are taken, i.e. we translate the set Π_r^{cube} by $\left(0,0,\frac{1}{2}\right)$ half of a $\mathbf{Z}_r^3$ unit 2^{-r}, "open it" at the upper face, and the resulting set is Π_r^{below}. This digitization scheme is also equivalent to translating the plane by half of a $\mathbf{Z}_r^3$ unit towards the xy-plane and rounding off z-values with respect to this unit.

This digitization scheme defines a *digital plane* as an r-grid point set

$$DIG_r^{below}(\alpha) = \left\{(i,j,k) \in \mathbf{Z}_r^3 : k = \lfloor ai + bj + c \rfloor_r \right\}$$

where $\lfloor u \rfloor_r$ is the greatest number in $\mathbf{Z}_r$ not larger than the real number u. This set is arbitrary sparse as a plane approaches vertical.

TASK: A non-vertical plane α has to be determined in the explicit form $z = a_0 x + b_0 y + c_0$ from the finite input set $\mathbf{G} \subset \mathbf{Z}_r^3$.

The input set $\mathbf{G}_r = DIG_r^{below}(\Theta)$ is a finite subset of a digital plane. Of course there are different planes α which may generate a set $\mathbf{G}_r$ in this way. Therefore a solution specifying the unknown ground truth α is not possible if only one input set $\mathbf{G}_r$ is given. But still we may be able to solve this task by calculating a unique solution α_r which converges towards α as the resolution increases, see Fig. 6. A distance measure on the set of all planes has to be defined for specifying convergence of planes. A convergent method for calculating such a sequence of planes α_r would be methodologically sound with respect to the soundness properties stated in Section 1.1. As a necessary condition the method should allow calculation of a unique solution α_r for given sets $\mathbf{G}_r$, for $r \geq r_0$.

The task may be generalised with respect to higher-order approximation faces. At first we discuss a specific aspect of this task: What is the minimum size of a set $\mathbf{G}_r$ which allows a certain calculation of an approximation plane?

The use of least-squares approximation allows us to specify a general method for calculating approximation planes based on discrete input data.

The use of a least-squares approximation techniques for representations of digital objects was proposed in [20]. In [21] it was proved that the *least-squares approximation straight-line* uniquely determines the digital straight-line where the input data are given for a certain digital interval.

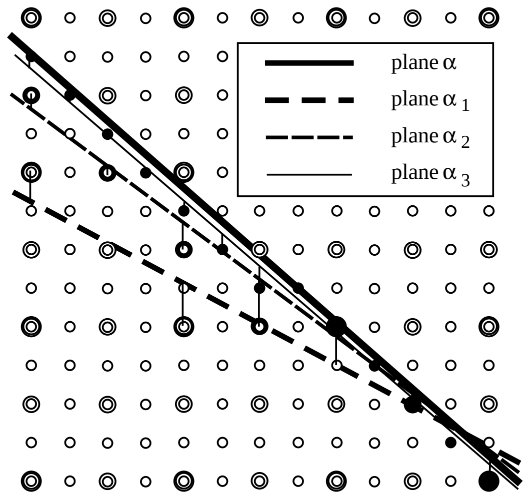

Fig. 6. A 2D sketch of three consecutive approximations of a given plane. The lowest resolution produces a plane supported by four sampling points, the next resolution level is based on seven sampling points, and the third resolution level is based on 13 samples, all below or on the given plane. The approximation planes will intersect the given plane somewhere in general.

We define the *least-squares approximation plane*

$$LSA_{plane}\left(\mathbf{G}_r\right)$$

for $\mathbf{G}_r$ to be a plane which minimizes the sum of the squares of the vertical distances to all points in $\mathbf{G}_r$. Note that this error measure is related to the assumed digitization model, and the resolution parameter r has impact on this measure by defining scaling and the sampling rate for the set Θ incident with α.

A method for determining such least-squares approximation planes is well-known from statistics, see, e.g. [1], where a general, not necessary digital input $\{(x_i, y_i, z_i) : i = 1, 2, ..., t\}$ is assumed. A comparison with an unknown ground truth is not relevant in statistics, and a discussion of different resolutions is also irrelevant in this general case. For such a general case assume that the equation of the least-squares approximation plane $LSA_{plane}\left(\mathbf{G}\right)$ is parameterized as $z = ax + by + c$. Then the error function

$$\Phi\left(\mathbf{G}; a, b, c\right) = \sum_{i=1}^{t} \left(ax_i + by_i + c - z_i\right)^2$$

has to be minimized. This traditional optimization problem is solved by obtaining the coefficients a, b, and c from the equation system

$$\frac{\partial \Phi}{\partial a} = 0, \quad \frac{\partial \Phi}{\partial b} = 0, \quad \text{and} \quad \frac{\partial \Phi}{\partial c} = 0,$$

i.e.

$$a \sum_{i=1}^{t} x_i^2 + b \sum_{i=1}^{t} x_i y_i + c \sum_{i=1}^{t} x_i = \sum_{i=1}^{t} x_i z_i,$$

$$a \sum_{i=1}^{t} x_i y_i + b \sum_{i=1}^{t} y_i^2 + c \sum_{i=1}^{t} y_i = \sum_{i=1}^{t} y_i z_i, \quad \text{and}$$

$$a \sum_{i=1}^{t} x_i + b \sum_{i=1}^{t} y_i + c \sum_{i=1}^{t} 1 = \sum_{i=1}^{t} z_i.$$

A unique solution exists whenever the determinant of this equation system is not zero. For example, if all points in $\mathbf{G}$ coincide with a straight line then the solution is not unique.

The special case of a digital input set $\mathbf{G}_r$ was studied in [12]. An r-grid point set $\mathbf{G}_r \subset \mathbf{Z}_r^3$ is a *digital quadrangle* if there exists a plane α in $\mathbf{R}^3$ and integers m and n such that

$$\mathbf{G}_r = \left\{ (i, j, k) : 2^{-r} \le i \le m \cdot 2^{-r} \wedge 2^{-r} \le j \le n \cdot 2^{-r} \wedge k = \lfloor ai + bj + c \rfloor_r \right\}.$$

The projection $proj_{1,2}(\mathbf{G}_r)$ of a digital quadrangle into the ij-plane is a rectangular set of r-grid points. As for Θ in general, there are different planes α satisfying this equation for a given digital quadrangle.

The coefficients

$$\sum_{i=1}^{t} 1, \quad \sum_{i=1}^{t} x_i, \quad \sum_{i=1}^{t} y_i, \quad \sum_{i=1}^{t} x_i^2, \quad \sum_{i=1}^{t} y_i^2, \quad \text{and} \quad \sum_{i=1}^{t} x_i y_i$$

of the general equation system can easily be calculated for the assumed input of a digital quadrangle. Let

$$M_{ab}(\mathbf{G}_r) = \sum_{(i,j,k(i,j)) \in \mathbf{G}_r} i^a \cdot j^b \cdot k(i,j)$$

be the *moment of order ab* of the set $\mathbf{G}_r$. This leads to a special form of this equation system:

$$\frac{nm(m-1)(2m-1)}{6} \cdot a + \frac{nm(n-1)(m-1)}{4} \cdot b + \frac{nm(m-1)}{2} \cdot c = M_{10}(\mathbf{G}_r),$$

$$\frac{nm(n-1)(m-1)}{4} \cdot a + \frac{nm(2n-1)(n-1)}{6} \cdot b + \frac{nm(n-1)}{2} \cdot c = M_{01}(\mathbf{G}_r),$$

and

$$\frac{nm(m-1)}{2} \cdot a + \frac{nm(n-1)}{2} \cdot b + nm \cdot c = M_{00}(\mathbf{G}_r).$$

This system has a determinant equal to

$$\left(n^2-1\right)\left(m^2-1\right)n^3m^3/144,$$

and so, for $n>1$ and $m>1$ the coefficients a, b, and c are uniquely determined.

Theorem 20. (LSA Uniqueness Theorem *[12]* **):** *Let* $\mathbf{G}_r \subset \mathbf{Z}_r^3$, $\mathbf{H}_r \subset \mathbf{Z}_r^3$, *with* $proj_{1,2}(\mathbf{G}_r) = proj_{1,2}(\mathbf{H}_r)$. *Assume that both sets contain at least three non-collinear* $r-$*grid points, and let* $LSA_{plane}(\mathbf{G}_r)$ *and* $LSA_{plane}(\mathbf{H}_r)$ *be the corresponding least-squares approximation planes. Then it holds that* $\mathbf{G}_r = \mathbf{H}_r$ *iff* $LSA_{plane}(\mathbf{G}_r) = LSA_{plane}(\mathbf{H}_r)$.

This result allows to define storage-efficient coding schemes for digital plane segments. In the context of this Section it may also support a possible way to answer the question about the soundness of the least-squares approximation approach.

Asuume a given set Θ with non-empty interior and incident with a plane α. It holds that for $r \geq r_0$, any input set $\mathbf{G}_r = DIG_r^{below}(\Theta)$ always contains at least three non-collinear $r-$grid points. Thus it holds that for $r \geq r_0$ the set $\mathbf{G}_r$ uniquely determines a plane $\alpha(\mathbf{G}_r) = \alpha_r$ with representation $z = a_r x + b_r y + c_r$. The plane α is assumed to be specified by $z = a_0 x + b_0 y + c_0$. We define the distance between such two planes by

$$d_{plane}(\alpha(\mathbf{G}_r), \alpha) = \sqrt{(a_r - a_0)^2 + (b_r - b_0)^2 + (c_r - c_0)^2}.$$

This measure d_{plane} is a metric on the set of all planes in $\mathbf{R}^3$.

Theorem 21. (LSA Convergence Theorem): *Asuume a given set* Θ *with non-empty interior and incident with a plane* α. *Then it holds that*

$$\lim_{r\to\infty} d_{plane}(\alpha_r, \alpha) = 0.$$

This Theorem follows from the equation system given above, and it even holds that

$$d_{plane}(\alpha, \alpha(\mathbf{G}_{r+1})) \leq d_{plane}(\alpha, \alpha(\mathbf{G}_r)),$$

for $r \geq r_0$. There are cases where

$$d_{plane}(\alpha, \alpha(\mathbf{G}_{r+1})) = d_{plane}(\alpha, \alpha(\mathbf{G}_r)),$$

see for example a plane α parallel to the xy-plane defined by $z = const \cdot 2^{-r_1}$ where *const* is an integer.

3.3 Integration of Jordan Face Gradients

There are many publications about numeric differentiations, but just a few publication about integration based on discrete input data, see [13].

We assume as input a finite set $\mathbf{P}_r$ of gradients $(p(x,y), q(x,y))^T \in \mathbf{R}^2$ at exactly all r-grid point positions in the interior of the base set

$$proj_{1,2}(\mathbf{C}_{uni}) = \left\{(x,y) \in \mathbf{R}^2 : \ 0 \leq x, y \leq N_0 + 1\right\}$$

of the universal cube $\mathbf{C}_{uni}$. This set is assumed to be a digital representation of one (!) measurable Jordan face $\mathbf{F} = \mathbf{F_B}(\varphi, \psi, \chi)$, for a certain resolution parameter r. For the sequence of finite grids $I(\mathbf{B}) \cap \mathbf{Z}_r^3$ it holds that

$$\lim_{r \to \infty} \left(I(\mathbf{B}) \cap \mathbf{Z}_r^3\right)$$

is dense in $\mathbf{B}$. W.l.o.g., let $\mathbf{B} = proj_{1,2}(\mathbf{C}_{uni})$, $x = \varphi(x,y)$, $y = \psi(x,y)$, and $z = \chi(x,y)$, i.e. the face is assumed to be in a position that allows a unique representation with respect to the xy-plane. It follows that

$$p(x,y) = \chi_x(x,y) = \frac{\partial \chi(x,y)}{\partial x} \quad \text{and} \quad q(x,y) = \chi_y(x,y) = \frac{\partial \chi(x,y)}{\partial y}.$$

The assumed input situation corresponds to a certain step in *shading based shape recovery*, see, e.g., [11], when at first gradients are calculated based on given radiance information, and surface recovery has still to be performed based on this intermediate gradient information. For this case the open set $I(\mathbf{B})$ may be considered to be the em image domain in the projection plane, and $z = \chi(x,y)$ denotes the *depth* of the surface points (roughly: the distance between the camera and the projected object surface) assuming *parallel projection* as the model of the image acquisition process. Based on this we may restrict the possible set of functions χ, e.g. forbidding unlimited numbers of oscillations as in

$$z = \chi(x,y) = \cos\left(\frac{1}{x}\right),$$

or "steep slopes" characterized by very high gradient magnitudes, or "very dynamic" depth values where the difference between minimum and maximum exceeds a reasonable threshold. However we state the basic task in general form:

TASK: The task is to calculate the face $\mathbf{F}$ based on the available input set $\mathbf{P}_r$ of gradients at r-grid point positions.

Integration is uniquely determined up to an additive constant what corresponds to a translation of function χ, i.e. only a *main function* χ_0 may be calculated with $z = \chi_0(x,y) + const$, but the global additive parameter $const$ remains unknown. Thus the task is actually that a differentiable main function χ_0 has to be calculated, and $const$, a global "shift in depth", can not be specified. In computer vision applications, this value $const$ can be estimated by triangulation techniques (a pair of corresponding points in binocular stereo images, a surface point illuminated by a laser point light source, etc.). Also note that we are not able to calculate explicit representations of an unknown face **F** in general. The face **F** can be the "visible surface of an scene object of arbitrary complexity". The goal is to generate all χ_0 values at all r-grid points in the open base set $I(\mathbf{B})$.

After this specification of the task, we first have to determine for which Jordan surfaces this problem of calculating χ_0 values based on gradient information is uniquely solvable. As a corollary of *Frobenius' Theorem* it holds that the *integrability condition*

$$p_y(x,y) = q_x(x,y)$$

has to be satisfied on **B** for the given vector field of gradients:

Theorem 22. (Face Integrability Theorem): *Let* $(p(x,y), q(x,y))^T$ *be a* $C^{(1)}(\mathbf{B})$ *-continuous vector field. Then there exists a* $C^{(2)}(\mathbf{B})$ *-continuous main function* $\chi(x,y)$ *with* $\chi_x = p$ *and* $\chi_y = q$ *on* **B** *iff* χ *satisfies the integrability condition on* **B**.

For example, the *Schwarz function*

$$\chi(x,y) = \begin{cases} \frac{xy\left(x^2-y^2\right)}{x^2+y^2}, & \text{if} \quad (x,y) \neq (0,0) \\ \quad 0 \quad , & \text{if} \quad (x,y) = (0,0) \end{cases}$$

does not satisfy the integrability condition in point $(0,0)$. Furthermore there are functions which satisfy the integrability condition, but which are not $C^{(2)}$ -continuous [11]. The measurable Jordan face $\mathbf{F} = \mathbf{F_B}(\chi)$ is defined to be integrable if χ is $C^{(2)}(\mathbf{B})$ -continuous.

Now let γ be a piecewise $C^{(1)}$ curve in the set **B**,

$$\gamma : \quad [a,b] \;\rightarrow\; \mathbf{R}^2, \quad \text{and} \quad \gamma(t) = (\gamma_1(t), \gamma_2(t)) = (x(t), y(t))$$

with $a < b$, $\gamma(a) = (x_0, y_0)$ and $\gamma(b) = (\bar{x}, \bar{y})$. For any curve of this kind and any integrable face **F** it holds that

$$\chi(\bar{x},\bar{y}) = \chi(x_0,y_0) + \int_\gamma p(x,y)\,dx + q(x,y)\;dy$$

$$= \chi(x_0,y_0) + \int_a^b [p(\gamma_1(t),\gamma_2(t)) \cdot \dot{\gamma}_1(t) + q(\gamma_1(t),\gamma_2(t)) \cdot \dot{\gamma}_2(t)]dt,$$

i.e. the result of the face function χ at position $(\bar{x},\bar{y})$ is independent of the chosen curve γ. However the chosen initial value $\chi(x_0,y_0)$ has influence.

Now we consider the digital case. The gradient values of face **F** are assumed to be given for grid point positions.

The "path integration model" has stimulated different local techniques for discrete integration. Furthermore a few global techniques were discussed for a fixed level of resolution, see [13].

For discussing the local techniques let us assume that for $r \geq 0$ the digital path

$$\mathbf{g}_r = \left[(x_1, y_1), (x_2, y_2), ..., \left(x_{(2^r(N_0+1)-1)^2}, y_{(2^r(N_0+1)-1)^2} \right) \right]$$

is a repetition free 4-connected path passing through exactly all $N_r \times N_r$ r-grid points in the open base set $I(\mathbf{B})$. For consecutive grid points (x_{t-1}, y_{t-1}), (x_t, y_t) in this path $\mathbf{g}_r$, for $2 \leq t \leq (2^r(N_0+1)-1)^2$, it is

$$\text{either} \quad dx_t = 2^{-r} \quad \text{and} \quad dy_t = 0, \quad \text{or} \quad dx_t = 0 \quad \text{and} \quad dy_t = 2^{-r},$$

where $x_t = x_{t-1} + dx_t$ and $y_t = y_{t-1} + dy_t$. Such a path may follow a certain general generation scheme, e.g., to be a meander, a Peano, or a Hilbert scan [26], and it may be considered to be a *digital sample* (e.g. by grid-intersection digitization) of a piecewise $C^{(1)}$ curve γ_r in the set $\mathbf{B}$, i.e. the curve γ_r has exactly all points listed in the digital path $\mathbf{g}_r$, as its digital image, i.e. all r-grid points in the open base set $I(\mathbf{B})$ in the order as specified by the given digitial path. W.l.o.g. we may also assume that $\mathbf{g}_r$ always starts (say with a "diagonal step") at

$$(x_1, y_1) = \left(2^{-r}, 2^{-r}\right)$$

and ends at, say (assume N_0 is even)

$$\left(x_{2^r(N_0+1)-1}, y_{2^r(N_0+1)-1}\right) = \left(N_0 + 1 - 2^{-r}, 2^{-r}\right).$$

This allows γ_r to start at $\gamma_r(a) = (0,0)$ in "one corner" of the base set $\mathbf{B}$, and leading to the corner $\gamma_r(b) = (N_0+1, 0)$. We assume that $z_0 = \chi(0,0)$ is given and take this value as a the initial depth value for the *discrete path integration*

$$\chi_r(x_s, y_s) = z_0 + \sum_{t=1}^{s} \left(p(x_t, y_t)\ dx_t + q(x_t, y_t)\ dy_t \right)$$

where point $(x_0, y_0) = (0,0)$ is assumed to be the start point of the path $\mathbf{g}_r$ for defining the initial step values dx_1 and dy_1.

The values dx_t and dy_t would be defined by a chosen digital path scheme, e.g. the meander, for grid resolution r.

Then the following question may be asked: Assume that $\mathbf{F} = \mathbf{F_B}(\chi)$ is an integrable face and $\mathbf{p}$ is any point in the open base set $I(\mathbf{B})$. For what classes of integrable faces and of discrete integration pathes we can state that for any $\varepsilon > 0$ there exists an integer r_ε and an r_ε-grid point $\mathbf{p}_\varepsilon$ in $I(\mathbf{B})$ such that $|\chi(\mathbf{p}) - \chi_{r_\varepsilon}(\mathbf{p}_\varepsilon)| < \varepsilon$?

All planar faces and any discrete integration path satisfy this statement.

A discrete path integration method satisfying this statement is sound with respect to convergence and convergence towards the proper value. The recent progress in shading based shape recovery (which leads to gradient information) is one argument for suggesting the study of such problems in local or global discrete integration. For practical applications a more detailed discussion of soundness properties may be of interest, as robustness with respect to noise, or with respect to "steep gradients" ("steep" in relation to the resolution r), see [13]. In this

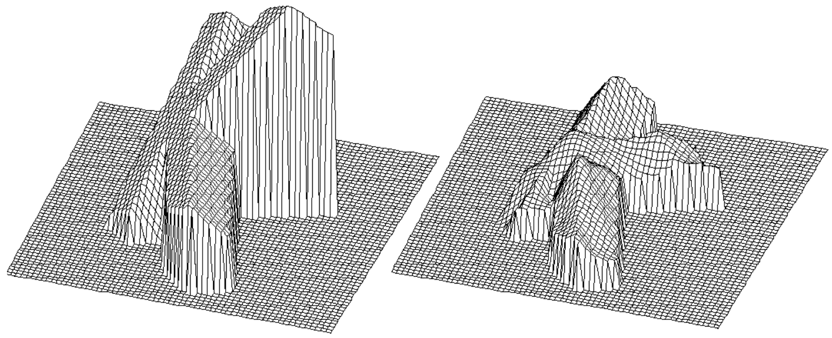

Fig. 7. A K-shaped synthetic polyhedron with a maximum height of 162.43 grid units (on the left). The maximum height error of the reconstructed surface (on the right) is equal to 90.94 grid units where the visualized height values are averages of four different discrete path integrations (i.e. integrations following four different digital paths), see [13].

paper it was shown that the discussed discrete path integration technique has drawbacks if the face $\mathbf{F} = \mathbf{F_B}(\chi)$ is more characterized by being a Jordan surface consisting of several planar faces (a "polyhedral object") instead of being a single integrable face, see Fig. 7. Of course, this corresponds to the Face Integrability Theorem as cited above.

3.4 Solution of a Cauchy Problem

As a final (and solved) task for discussing the stated soundness properties of geometric algorithms based on gridding techniques we consider a special Cauchy problem. We assume as discrete input a collection of image data $E(x, y)$ at exactly all r-grid point positions in the 2D interior $I(\mathbf{B})$ of the base set of the universal cube $\mathbf{C}_{uni}$. These image intensities are assumed to correspond to reflectance properties of the projected object surfaces according to a certain reflectance model. Assuming a linear reflectance model this leads to the (transformed) *linear image irradiance equation*

$$a\frac{\partial\chi}{\partial x}(x, y) + b\frac{\partial\chi}{\partial y}(x, y) = E(x, y),$$

which was studied in [15, 16]. As in Section 3.3 before we assume a measurable Jordan face $\mathbf{F} = \mathbf{F_B}(\chi)$ defined on set $\mathbf{B}$ where the values of the depth function χ are assumed to be known at some boundary points of $\mathbf{B}$ (*boundary condition*).

The function E is assumed to be integrable on $\mathbf{B}$, and let $(a,b) \neq (0,0)$.

TASK: The task is to calculate the face $\mathbf{F}$ based on the available input set of irradiance values $E(x,y)$ at r-grid point positions, and based on a specified boundary condition, where the face satisfies the linear image irradiance equation.

More precisely, we are interested in a numerical solution of the following *Cauchy problem*: The face function χ is assumed to be integrable on base set $\mathbf{B}$. If $sgn(ab) \geq 0$ then

$$\chi(x,0) = f(x), \quad \text{for} \quad 0 \leq x \leq N_0 + 1$$

is given as boundary condition, and if $sgn(ab) < 0$ then

$$\chi(x, N_0+1) = f(x), \quad \text{for} \quad 0 \leq x \leq N_0 + 1$$

is given. Furthermore also

$$\chi(0,y) = g(y), \quad \text{for} \quad 0 \leq y \leq N_0 + 1$$

is assumed to be known. The functions f, g are integrable on $[0, N_0+1]$ and satisfy $f(0) = g(0)$ if $sgn(ab) \geq 0$, or $f(0) = g(N_0+1)$ if $sgn(ab) < 0$.

This Cauchy problem is given in "digital form", i.e. only values at r-grid point positions are given for functions $p = \chi_x$, $q = \chi_y$, E, f, and g.

For solving linear partial differential equations with the aid of the finite difference method see [31], Chapter 1. As mentioned before in Section 3.3 it holds that

$$\lim_{r \to \infty} \left(I(\mathbf{B}) \cap \mathbf{Z}_r^3 \right)$$

is dense in $\mathbf{B}$. Assuming normed function spaces on $\mathbf{B}$ this sequence of grids allows us to define corresponding normed grid spaces, defined on subsets of $\mathbf{B} \cap \mathbf{Z}_r^3$, for functions defined on r-grid points, see [15, 16] for details. A *finite difference scheme* (FDS) is defined for all grids $\mathbf{B} \cap \mathbf{Z}_r^3$ of different resolution, for $r = 0, 1, 2, ...,$ and basically it characterizes an operator R_r mapping an unknown function defined on $\mathbf{B}$, as χ in our case, into a function χ_r,

$$R_r(\chi) = \chi_r, \quad \text{with} \quad \chi_r(i,j) \approx \chi\left(i \cdot 2^{-r}, j \cdot 2^{-r}\right)$$

defined on r-grid points which is considered to be an approximation of the unknown function.

For example, applying a (simple) *forward difference approach* together with Taylor's expansion yields

$$\left.\frac{\partial \chi}{\partial x}\right|_r^{(i,j)} = \frac{\chi_r(i+1,j) - \chi(i,j)}{2^{-r}} + O\left(2^{-r}\right)$$

in the x-direction, and

$$\left.\frac{\partial \chi}{\partial y}\right|_r^{(i,j)} = \frac{\chi_r(i,j+1) - \chi(i,j)}{2^{-r}} + O\left(2^{-r}\right)$$

in the y-direction. A (simple) *backward difference approach* in x-direction is given by

$$\left.\frac{\partial \chi}{\partial x}\right|_{r}^{(i,j)} = \frac{\chi(i,j) - \chi(i-1,j)}{2^{-r}} + O\left(2^{-r}\right),$$

just to mention a further example. The differences are normalized by the distance 2^{-r} between neighboring r-grid points, in x- or in y-direction. Larger neighborhoods could be used for defining more complex forward or backward approaches, and further approaches may also be based on symmetric, or unbalanced neighborhoods of r-grid points. Finally, a finite difference scheme is characterized by selecting one approach for the $x-$, and an other one for the y-direction.

The *forward-forward FDS* transforms the given differential equation into

$$a \cdot \frac{\chi_r(i+1,j) - \chi_r(i,j)}{2^{-r}} + b \cdot \frac{\chi_r(i,j+1) - \chi_r(i,j)}{2^{-r}} + O\left(2^{-r}\right) = E\left(i2^{-r}, j2^{-r}\right),$$

and this equation may be simplified as

$$\tilde{\chi}_r(i,j+1) = \left(1 + \tfrac{a}{b}\right) \cdot \tilde{\chi}_r(i,j) - \tfrac{a}{b} \cdot \tilde{\chi}_r(i+1,j) + \tfrac{2^{-r}}{b} \cdot E\left(i2^{-r}, j2^{-r}\right),$$

where $\tilde{\chi}_r(i,j)$ is used as an approximation for function $\chi_r(i,j)$. The *backward-forward FDS* leads to

$$\tilde{\chi}_r(i,j+1) = \left(1 - \tfrac{a}{b}\right) \cdot \tilde{\chi}_r(i,j) + \tfrac{a}{b} \cdot \tilde{\chi}_r(i-1,j) + \tfrac{2^{-r}}{b} \cdot E\left(i2^{-r}, j2^{-r}\right),$$

the *forward-backward FDS* leads to

$$\tilde{\chi}_r(i+1,j) = \left(1 - \tfrac{b}{a}\right) \cdot \tilde{\chi}_r(i,j) + \tfrac{b}{a} \cdot \tilde{\chi}_r(i,j-1) + \tfrac{2^{-r}}{a} \cdot E\left(i2^{-r}, j2^{-r}\right),$$

and the *backward-backward FDS* leads to

$$\tilde{\chi}_r(i,j) = \tfrac{1}{1+c} \cdot \tilde{\chi}_r(i,j-1) + \tfrac{c}{1+c} \cdot \tilde{\chi}_r(i-1,j) + \tfrac{2^{-r}}{b(1+c)} \cdot E\left(i2^{-r}, j2^{-r}\right),$$

where $c = \frac{a}{b} \neq -1$, and to

$$\tilde{\chi}_r(i-1,j) = \tilde{\chi}_r(i,j-1) + \tfrac{2^{-r}}{b} \cdot E\left(i2^{-r}, j2^{-r}\right)$$

otherwise for $c = -1$. These schemes were studied in [15, 16].

A finite difference scheme is *consistent* with an initial boundary value problem if the error of approximation in representing the original problem converges to zero as $2^{-r} \to 0$. The listed four schemes are consistent.

A finite difference scheme is *convergent* to the solution χ_r (if it exists) if the digitization error converges to zero as $2^{-r} \to 0$. A further notion of stability for linear difference schemes was defined by *Rjabenki* and *Filippov*, see [31]. A linear difference scheme is *RF stable* if the operators

$$\left\{R_r^{-1}\right\}_{r=0,1,2,\ldots}$$

are *uniformly bounded* as $2^{-r} \to 0$.

Theorem 23. (General FDS Convergence Theorem *[31], Theorem 5.1* **):** *A consistent and RF stable finite difference scheme is convergent to the solution of the given Cauchy problem if such a solution exists.*

For the convergence analysis of the given schemes let $c = \frac{a}{b}$ assuming that $b \neq 0$, and $d = \frac{b}{a}$ assuming that $a \neq 0$.

Theorem 24. (FDS RF Stability Theorem *[15]* **):** *The forward-forward FDS is RF stable iff $-1 \leq c \leq 0$. The backward-forward FDS is RF stable iff $0 \leq c \leq 1$. The forward-backward FDS is RF stable iff $0 \leq d \leq 1$. The backward-backward FDS is RF stable iff $c \geq 0$ or $c = -1$.*

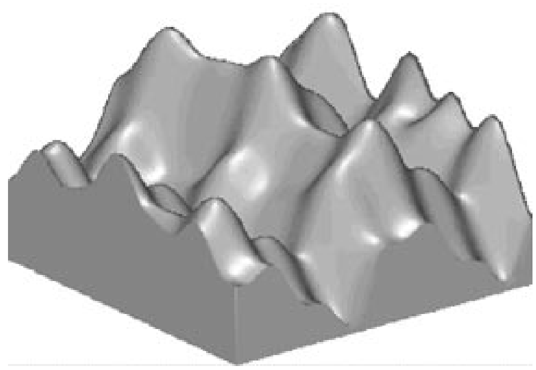

Fig. 8. An example of a suggested function for testing different surface techniques [2].

Consequently (by the General FDS Convergence Theorem), in these positive cases the sequences of functions

$$\{\tilde{\chi}_r\}_{r=0,1,2,\ldots}$$

are convergent to the solution of the specified Cauchy problem. A few illustrations of shape recovery results were visualized in [15, 16] for synthetic input functions χ as the *volcano*

$$\chi_{volcano}(x,y) = 1 \Big/ \left(4\left(1 + \left(1 - x^2 - y^2\right)^2\right)\right)$$

and the *mountain*

$$\chi_{mountain}(x,y) = 1 \Big/ \left(2\left(1 + x^2 + y^2\right)^2\right)$$

where it was assumed that the shading values on these Jordan faces satisfy the linear image irradiance equation. A more complex function,

$$\chi_{hills}(x,y) = \frac{\sin(3x)^4 + \cos(2y)^4 + \sin(x+4y)^3 - \cos(xy)^5}{2} + 1,$$

is shown in Fig. 8.

Such functions may define a certain testbed for a more detailed comparison of the behavior of the different surface recovery techniques as the minimum Jordan surface calculation assuming a certain digitization method, the approximation of faces assuming a certain predefined explicit analytic shape, the recovery based on gradients generating gradients based on numeric differentiation, or the recovery based on solutions of differential equation systems assuming a specific object-surface reflectance model.

4 Conclusions

Fundamental approaches "How to define a 3D surface?", "How to approximate discrete surface points?", "How to perform discrete integration?", or "How to solve a linear differential equation system based on discrete input data?" were discussed with respect to possible improvements if new technologies allow higher grid resolutions. Such discussions and related results might be of interest for re-considering some established approaches in digital geometry. For example, [30], property 1, define a *Jordan boundary* as a set which satisfies the Jordan surface theorem in 3D space. Their boundary tracking algorithm for boundary faces of the cells of a given 3D grid point set may be used for sound volume calculations, but not for sound surface area calculations. A *near-Jordanness property* (in short: every path from an element in the interior to an element of the exterior exits through the given set of polygons), see e.g. [6], was used in recent publications of *G. Herman, J. K. Udupa et al.* for discussing the partition of the digital space into an inside and an outside. A Jordan surface of a 6-connected cellular complex [9] satisfies the Jordan surface theorem because it is just a special case of a Jordan surface. It was proved, see [6], that the near-Jordanness property is useful for discussing algorithmic approaches for digital spaces.

The same soundness criterion was discussed for four different situations. In three cases we can state that the problem (i.e. defining a technique, and proving that this technique satisfies the soundness properties) is solved. Finding sound techniques for solving the discrete integration problem seems to be of fundamental complexity. However, the discussed "discrete surface problem" and "discrete Cauchy problem" might be compared at complexity level, and both problems were solved already.

The calculation of features of digital objects defined by voxel sets is certainly a topic in digital geometry. However the first example, the Jordan surface problem, should already point out that a model in continuous mathematics may help to propose a sound approach for feature calculation. The next examples did lead more and more away from the digital geometric case, ending with the study of a Cauchy problem at a numerical or analytical level of mathematics. However, in all these cases gridding techniques are or should be applied. As a general hypothesis this leads to the opinion that different geometric approaches relevant to 3D object analysis will increasingly interact in the future. This is also expected at the computational level.

Recent interest in computational geometry develops also towards the study of efficacy (i.e. robustness or numerical stability) of geometric algorithms, see [17]. The studied soundness constraints might be interpreted in this direction. The calculation of the minimum Jordan surface (Section 3.1) should be of high interest in this area. The calculation of the least-squares approximation plane (Section 3.2) belongs obviously to the class of geometric optimization problems, also studied in computational geometry. However, in [17] only the 2D case of polygonal curve approximation is cited in this class, and not this 3D computational problem. The gradient based recovery approach (Section 3.3) may also lead to interesting computational questions if combined with accuracy or approximation constraints.

The 3D shape description and recovery problem, based on digital input data, is a very multi-disciplinary problem. CAD systems apply a broad variety of digital surface representation techniques. Gridding techniques for differential equations, as briefly discussed in Section 3.4, are also studied in computational physics, see [35] - just to cite two fields different from 3D image analysis.

Acknowledgment
The co-authors of joint publications to topics sketched in this report are *Jovisa Zunic* (Yugoslavia), *Ivan Stojmenovic* (Canada), *Karsten Schlüns* (New Zealand), and *Ryszard Kozera* (Australia). *Fridrich Sloboda* (Slovakia) made substantial contributions towards the subject sketched in Section 3.1 during his stay at CITR Tamaki. I thank my colleague *Richard Lobb*, and *Fridrich Sloboda* for commenting on the initial draft of this report.

References

1. I. W. Burr, *Applied Statistical Methods*, Academic Press, New York, 1974.
2. S. L. Cheng, Estimation of volume and surface area from isosurface, Postgraduate project in computer science, 415.780 FC, University of Auckland, 1997.
3. F. Guliak, Volume and surface area measurement of viable chondrocytes in situ using geometric modelling of serial confocal sections, *J. of Microscopy*, **173** ,1994, 245–256.
4. A. Jonas, N. Kiryati, Digital representation schemes for 3-d curves, CC Pub #114, July 1995, Dep. of Electrical Engineering, Technion - Israel Institute of Technology.
5. W. Heiden, T. Goetze, J. Brickmann, 'Marching cube Algorithmen zur schnellen Generierung von Isoflchen auf der Basis dreidimensionaler Datenfelder, in: *Visualisierung von Volumendaten*, Springer, Berlin, 1991, 112–117.
6. G. T. Herman, E. Zhao, Jordan surfaces in simply connected digital spaces, http://www.unipissing.ca/topology/p/a/a/z/06.htm, Topology Atlas Preprint #54, 1996.

7. S. Hoek, Generation of 3D cellular complexes with known ground truth, Postgraduate project in computer science, 415.705 ST, University of Auckland, 1997.
8. C. E. Kim, Three-dimensional digital line segments, *IEEE Trans. Pattern Anal. Mach. Intell.*, **PAMI-5**, 1983, 231–234.
9. R. Klette, M-dimensional cellular spaces, CAR-TR-6, Univ. of Maryland, Center for Automation Research, College Park, August 1983.
10. R. Klette, The m-dimensional grid point space, it CVGIP, **30**, 1985, 1–12.
11. R. Klette, A. Koschan, K. Schlüns, *Computer Vision - Räumliche Information aus digitalen Bildern*, Braunschweig, Vieweg 1996.
12. R. Klette, I. Stojmenovič, J. Žunić, A parametrization of digital planes by least-squares fits and generalisations, *Graphical Models and Image Processing*, **58**, 1996, 295–300.
13. R. Klette, K. Schlüns, Height data from gradient fields, Proc. *Machine Vision Applications, Architectures, and Systems Integration V*, SPIE 2908, Boston, Massachusetts, Nov. 18-19, 1996, 204–215.
14. J. Koplowitz, On the performance of chain codes for quantization of line drawings, *IEEE Trans. Pattern Anal. Mach. Intell.*, **PAMI-3**, 1981, 180–185.
15. R. Kozera, R. Klette, Finite difference based algorithms for linear shape from shading, *Machine Graphics & Vision*, 1997 (to appear).
16. R. Kozera, R. Klette, Evaluation of finite difference algorithms for a linear shape from shading problem, Proceed. *Advances of Visual Form Analysis*, Capri, Italy, World Scientific, 1997, 330–339.
17. D. T. Lee, Computational geometry, *ACM Computing Surveys*, **28**, 1996, 27–31.
18. W. E. Lorensen, H. E. Cline, Marching cubes: a high resolution 3D surface construction algorithm, *Computer Graphics*, **21**, 1987, 163–169.
19. H. v. Mangoldt, K. Knopp, *Einführung in die höhere Mathematik, III. Band, 12. Auflage*, Leipzig, S. Hirzel Verlag, 1965.
20. R. A. Melter, A. Rosenfeld, New views of linearity and connectedness in digital geometry, *Pattern Recognition Lett.*, **10**, 1989, 9–16.
21. R. A. Melter, I. Stojmenovič, J. Žunić, A new characterization of digital lines by least square fits, *Pattern Recognition Lett.*, **14**, 1993, 83–88.
22. J. C. Roberts, An overview of rendering from volume data including surface and volume rendering, University of Kent at Canterbury, TR, December 1993.
23. A. Rosenfeld, A. C. Kak, *Digital Image Processing (2nd ed.)*, Academic Press, New York, 1982.
24. A. Rosenfeld, Digital geometry - a bibliography, in: Advances in Digital and Computational Geometry (eds: R. Klette, A. Rosenfeld, F. Sloboda), Springer, Singapore (to appear).
25. W. Scherer, Ein Satz über Gitter und Volumen, *Mathematische Annalen*, **86**, 1922, 99–107.
26. W. Skarbek, Generalized Hilbert scan in image printing, in: *Theoretical Foundations of Computer Vision* (R. Klette, W. Kropatsch, eds.), Akademie Verlag, Berlin, 1992, 47–58.
27. F. Sloboda, B. Zaťko, Piecewise linear approximation of planar Jordan curves and arcs: theory and applications, in: *Computing Supplement*, **11**, (W. Kropatsch, R. Klette, F. Solina, eds.), Springer, Wien, 1996, 183–200.
28. F. Sloboda, B. Zaťko, J. Stoer, On approximation of planar one-dimensional continua, in: Advances in Digital and Computational Geometry (eds: R. Klette, A. Rosenfeld, F. Sloboda), Springer, Singapore (to appear).

29. F. Sloboda, On approximation of Jordan surfaces: a topological approach, Internal Memo, CITR group, Tamaki, The University of Auckland, May 1997.
30. J. K. Udupa, V. G. Ajjanagadde, Boundary and object labelling in three-dimensional images, *CVGIP*, **51**, 1990, 355–369.
31. P. J. Van der Houwen, Finite difference methods for solving partial differential equations, Mathematical Centre Tracts 20, Mathematisch Centrum Amsterdam 1968.
32. K. Voss, *Discrete Images, Objects, and Functions in* Z^n. Berlin, Springer, 1993.
33. J. Wilhelms, A. V. Gelder, Topological considerations in isosurface generation, Baskin Center for Computer Engineering and Information Sciences, University of California, Santa Cruz, 1994, UCSC-CRL-94-31.
34. G. Wyvill, C. McPheeters, B. Wyvill, Data structures for soft objects, *The Visual Computer*, **2,** 1986, 227–234.
35. D. P. Young, R. G. Melvin, M. B. Bieterman, A locally refined rectangular grid finite element method: application to computational fluid dynamics and computational physics, *J. of Comp. Physics*, **92**, 1991, 1–42.

This article was processed using the LaTeX macro package with LLNCS style